IEICE TRANS. INF. & SYST., VOL.E98–D, NO.3 MARCH 2015

LETTER

No-Reference Blur Strength Estimation Based on Spectral Analysis of Blurred Images*

Hanhoon PARK[†a)], ***Member***

SUMMARY In this letter, we propose a new no-reference blur estimation method in the frequency domain. It is based on computing the cumulative distribution function (CDF) of the Fourier transform spectrum of the blurred image and analyzing the relationship between its shape and the blur strength. From the analysis, we propose and evaluate six curve-shaped analytic metrics for estimating blur strength. Also, we employ an SVM-based learning scheme to improve the accuracy and robustness of the proposed metrics. In our experiments on Gaussian blurred images, one of the six metrics outperformed the others and the standard deviation values between 0 and 6 could be estimated with an estimation error of 0.31 on average.

key words: *no-reference, blur estimation, Fourier transform, cumulative distribution function, SVM*

1. Introduction

Image blur is a common problem in optical engineering and may be due to the point spread function or motion of the camera sensors. Thus, blur measurement has been a key technique in a number of applications such as image quality assessment [1]–[3], image restoration/enhancement [4], image segmentation [5], and camera intrinsic/extrinsic parameter estimation [6]. In the literature, a number of effective methods or metrics have been reported. They can be categorized into full-reference (FR) ones and no-reference (NR) ones. FR blur metrics generally require a reference (an original or perfect image) and work by comparing it against blurred images. NR blur metrics require no reference and generally work by analyzing the contents of blurred images with some heuristics or prior knowledge such as statistics of edge sharpness. Therefore, FR blur metrics are simple and easy to implement, and their accuracy is higher than that of NR blur metrics. However, in most real-world applications, the reference is unavailable. NR blur metrics are therefore ideally suited for real-world applications, and we are interested in NR blur metrics. NR blur metrics are usually divided into two groups: one is built in the spatial domain (NR-S) [1] and the other in the frequency domain (NR-F) [2]. In this letter, we try to develop a new NR-F blur metric for to the following reasons:

- NR-F blur metrics work more efficiently with large images.
- The blur model and process are more easily understood and implemented in the frequency domain.
- More interpretable blur-concerned information is observable in the frequency domain, which is unseen in the spatial domain. This provides insights on a new blur metric.

In Sect. 3, we will evaluate the efficiency of NR-F metrics against NR-S metrics.

Our metric is inspired by previous work [2] based on analyzing the cumulative distribution function (CDF) of the Fourier transform (FT) spectrum of an image. But in our metric, the CDF is computed in a slightly different way. Furthermore, unlike the previous work focused on detecting blurred images [2], our metric focuses on measuring the amount (or strength) of blur.

In fact, our metric is based on the well-known characteristics that the blur image has much energy in the lower frequency range and smaller energy in the higher frequency range. However, there is no sure metric to quantify such characteristics. Therefore, this letter aims to propose such a metric and the novelty of our metric lies in its effectiveness in measuring the energy with the purpose of accurately estimating the blur strength. Also, to our knowledge, such a metric that attempts to analyze the whole FT-CDF itself is not found in the existing NR-F metrics [7].

2. A New NR-F Blur Metric

2.1 Blur Model

In general, image blur can be modeled by 2D convolution between the input image $\mathbf{f}$ and a blur kernel $\mathbf{h}$ as follows.

$$\mathbf{g}(\mathbf{x}) = \mathbf{h}(\mathbf{x}) * \mathbf{f}(\mathbf{x}) + \mathbf{n}(\mathbf{x}), \tag{1}$$

where $\mathbf{n}$ represents the additive noise. This model is also used in this letter but it is assumed that there is no additive noise.

2.2 CDF

In this letter, the method of computing the CDF is slightly different from that described in the previous paper [2]. Given a blurred image $\mathbf{g}$, its spectrum image $\mathbf{S}$ is obtained by FT as

$$\mathbf{S} = \log\left(\mathbf{1} + \sqrt{Re\left(\mathcal{F}(\mathbf{g})\right)^2 + Im\left(\mathcal{F}(\mathbf{g})\right)^2}\right). \tag{2}$$

Manuscript received August 22, 2014.
Manuscript revised November 14, 2014.
Manuscript publicized December 19, 2014.

[†]The author is with Pukyong National University, Busan, 608–737 Korea.

*This study was funded by KARI.

a) E-mail: hanhoon_park@pknu.ac.kr

DOI: 10.1587/transinf.2014EDL8175

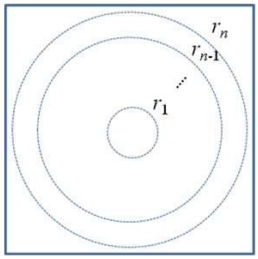

Fig. 1 Concentric rings on a spectrum image.

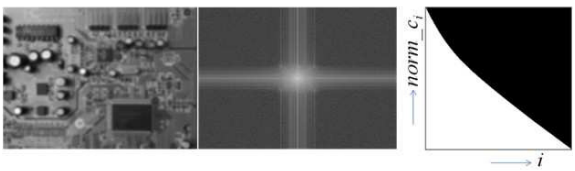

Fig. 2 Spectrum and CDF of a Gaussian blurred image.

Here, $Re()^2$ and $Im()^2$ are element-wise operations. The origin of the spectrum is moved to the center of the spectrum image. Next, supposing that there are n rings overlaid on the spectrum image as shown in Fig. 1, the spectrum values are averaged in each ring as

$$s_i = \frac{1}{N_i} \sum_{j=1}^{N_i} \mathbf{S}(\mathbf{x}_j), \qquad \mathbf{x}_j \in r_i, 1 \le i \le n. \tag{3}$$

Here, N_i is the number of pixels $\mathbf{x}_j$ overlapped with r_i. This computation is different from [2] where the spectrum values were just summed. Since the number of pixels in each ring is different from each other, the averaging computation can obtain more accurate spectrum values in each sub-band. Then, letting c_i be the cumulative sum of s_i,

$$c_i = \sum_{j=1}^{n-(i-1)} s_{n-(j-1)}, \qquad 1 \le i \le n. \tag{4}$$

Finally, c_i is normalized to a range between 0 and 1 as

$$norm\_c_i = \frac{c_i}{c_1}, \qquad 1 \le i \le n. \tag{5}$$

The resulting $norm\_c_i$ is the CDF value used in this letter. An example is shown in Fig. 2.

2.3 Measurement of Blur Strengths

As shown in Fig. 2, the CDF envelope curves of blurred images have concave shapes. This is because blurring has an effect of decreasing high frequency components whereas increasing low frequency components. The amount of increase or decrease depends on the blur strength (In this letter, blur strength indicates the standard deviation for Gaussian blur or the averaging filter size for motion blur). Therefore, there is an interesting tendency in the shapes of CDF envelope curves according to blur strengths, which is the main motivation of this study. Specifically, as depicted in

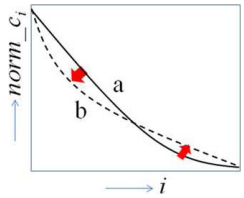

Fig. 3 CDF shape with a different amount of blur. *a*: weak blur, *b*: strong blur.

Fig. 3, as the blur strength increases, the envelope curve shape tends to change from *a* to *b*. From this observation, we can come up with some curve-shape analytic metrics useful for estimating the blur strength applied. However, it is difficult to predict what metric is the best. In this letter, we examine the following simple metrics[†]:

- $M1$: Finding the point ($a_{0.5}$ for the curve a in Fig. 4 (a)) where the CDF value becomes lower than 0.5,
- $M2s$: Dividing into two regions with a same width and calculating the difference (a_{rd} in Fig. 4 (b)) of two region areas, which is similar to the metric proposed in [2],
- $M2a$: Calculating the area below the envelope curve, i.e., calculating the sum of two areas (a_{ra} in Fig. 4 (b)), which is the same as the spectral metric of [9],
- $M3$: Fitting a straight line to the envelope curve points (i, $norm\_c_i$) and calculating the line slope (a_s in Fig. 4 (c)),
- $M4$: Halving the envelope curve, fitting straight lines to the half curve points, and calculating the difference (a_{ld} in Fig. 4 (d)) of two line slopes,
- $M5$: Finding the farthest point (a_{max} in Fig. 4 (e)) from a straight line c and computing $1/a_{max}$.

2.4 Learning the Measurements

From the preliminary experiments, we could know that:

- The measurement results depend on the CDF image size.
- The measurement results are not in a linear relationship with the blur strengths but a nonlinear relationship as shown in Fig. 5.
- The measurement results depend on the contents of original images as described in the previous paper [2].

Although the errors caused by the difference in the CDF image size can be compensated by rescaling the results with the size or by pre-normalizing CDF images to a fixed size, the others not. Therefore, to accurately measure the blur strengths, we use a supervised learning scheme. That is, after obtaining the measurement results from a number of images having different blur strengths and contents, the relationship between the blur strengths applied and their measurements is learned by using a support vector machine

[†]They are partially related to the Kolmogorov-Smirnov test [8].

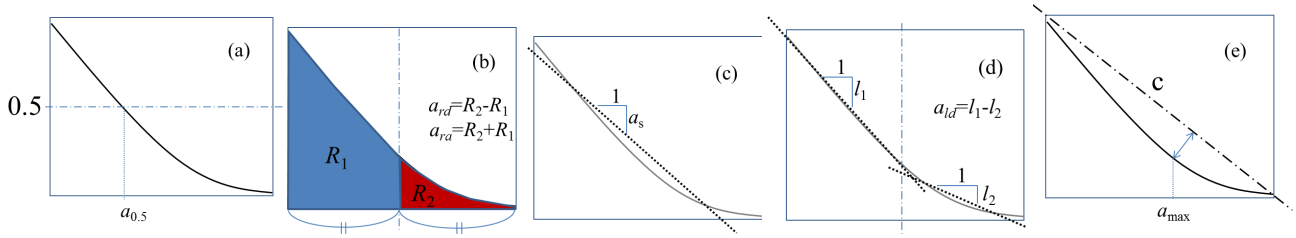

Fig. 4 CDF shape analysis for blur strength measurement. In (c) and (d), the straight dot lines are the fitted lines. In (e), c is a straight line connecting two corners (left top and right bottom) of CDF image.

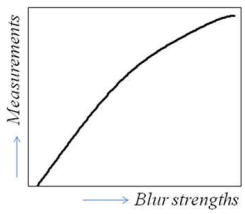

Fig. 5 The relationship between blur strengths applied and their measurements.

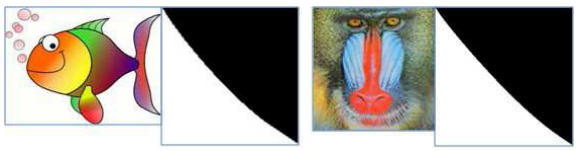

Fig. 6 CDF comparison of two different images.

Fig. 7 A part of images used in experiments.

(SVM) [10]. Then, the learned machine is used to map the measurements to the blur strengths.

Note that the dependency on the image contents is not a tricky problem. As shown in Fig. 6, the CDF images of two images having quite different contents are very similar and both have the same tendency as depicted in Fig. 3. Therefore, the dependency can be resolved by a learning scheme.

3. Experimental Results and Discussion

To evaluate the proposed metrics, the images of the LIVE database [11] were used (see Fig. 7). The database includes various clear scene images and their Gaussian blurred versions. At first, the uncorrupted images were corrupted by defocusing blur, i.e., the Gaussian blur with strengths (= standard deviations) of $\sigma = 0.3 * \{0.5 * f - 1\} + 0.8$, $(f = 3, 5, 7, \cdots, 35)$, using the *cvSmooth* function [12]. After computing the CDF images from the corrupted images using the method explained in Sect. 2.1, the blur strength-related measurements were obtained by using the six metrics in Sect. 2.2. Then, the mapping from the measurements to the blur strengths applied was learned using a multi-class SVM with a RBF kernel [10]. Finally, for the images corrupted by the Gaussian blur with known σ_Gs in the LIVE database, we followed the same processes and estimated the σ_Es using the SVM and compared them with the σ_Gs. In this letter, we omitted the results for motion blur because the metrics worked the same way for images with motion blur. However, we can partially predict the results for motion blurred images in Fig. 8 where we can know that the observation depicted in Fig. 3 is workable for motion blurred images as well.

Note that σ has 17 different values in our experiments (0.95, 1.25, $\cdots$, 5.75). Therefore, the SVM classified the measurements from six metrics into 17 classes (CL_1, CL_2, $\cdots$, CL_{17}). It indicates that the blur strengths are estimated roughly. For example, if σ_G is 2.166638, it is mapped to the class ($\sigma_E = 2.15$). In addition, the blur strength difference between the classes is 0.3. It indicates that if the difference in blur strengths is smaller than 0.3, it may not be recognized correctly. For example, if σ_Gs are 1.708303 and 1.851533, both are mapped to the same class ($\sigma_E = 1.85$). The images having σ_G larger than 6.0 were excluded. In this letter, if the classification is correct, it is considered that the blur strength estimation is successfully done.

Table 1 shows the estimation error of six metrics, i.e., $|\sigma_G - \sigma_E|$. Figure 9 shows the estimation results of each metric for some images. It seemed that only $M2s$ and $M3$ play a role as a blur metric. That is, as σ_G increases, σ_E monotonically increases. Also in terms of estimation error, the metrics $M2s$ and $M3$ were better than the others. $M3$ was the best. The estimation results of $M3$ were very similar to the true blur strengths except for the cases that σ_G is larger than 6.0 as in the results of "Paintedhouse" images. The estimation error of $M3$ was 0.31 on average. It indicates that the SVM has a misclassification distance of 1 on average. Here, the misclassification distance is the index difference between the estimated class (CL_i) and the true class (CL_j), i.e., $|i - j|$. Therefore, if the increment of f values becomes smaller than 2, the error could be further reduced.

Although the computation time of $M3$ is longer than the others, it is still very short (see Table 2). Since the other processes including spectrum and CDF computation took about 40ms, all the metrics worked within 41 ms in an ordinary laptop computer with 1.9GHz A8-4500M APU and 4GB RAM.

Finally, to show the efficiency our NR-F metric against NR-S metrics, a NR-S metric which was proposed by Park

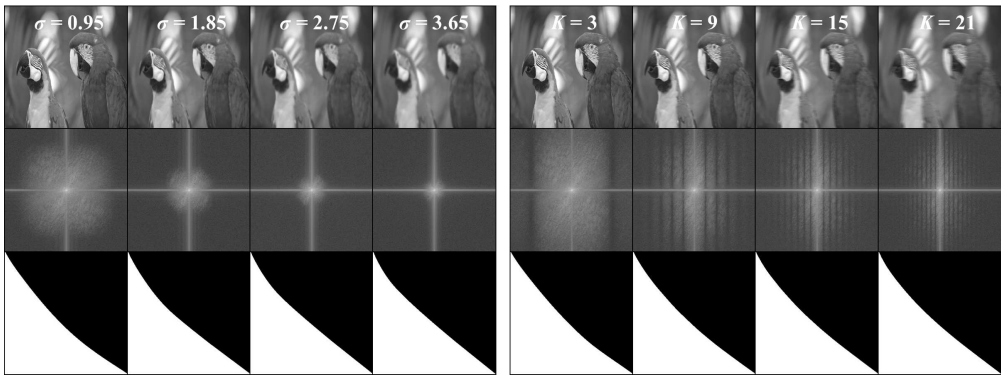

Fig. 8 CDF shape with a different amount of Gaussian and motion blur. Top row: input blurred images, middle row: spectrum images, and bottom row: CDF images. The motion blur was added using a 1-D horizontal averaging filter $\frac{1}{K}[1\ 1\ \ldots\ 1]$, where K is the kernel size. We can observe the same shape-changing aspect of CDF curve for both Gaussian and motion blur.

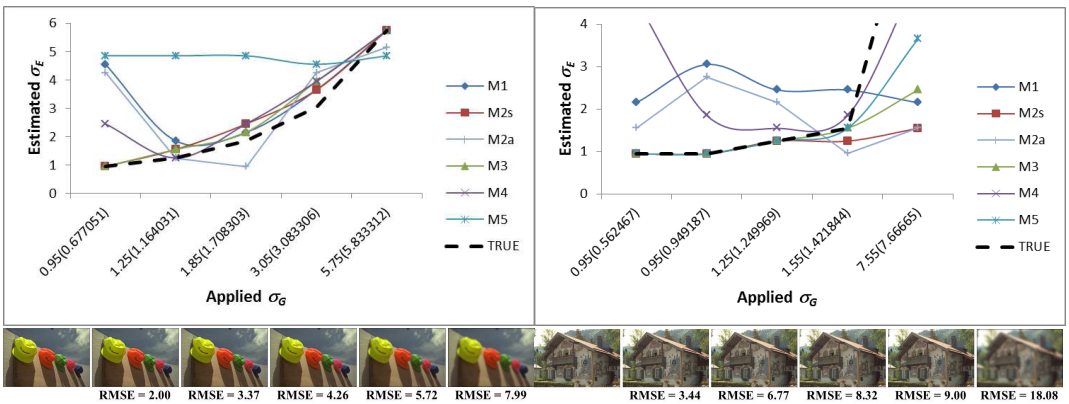

(a) "Caps" and "Paintedhouse" images

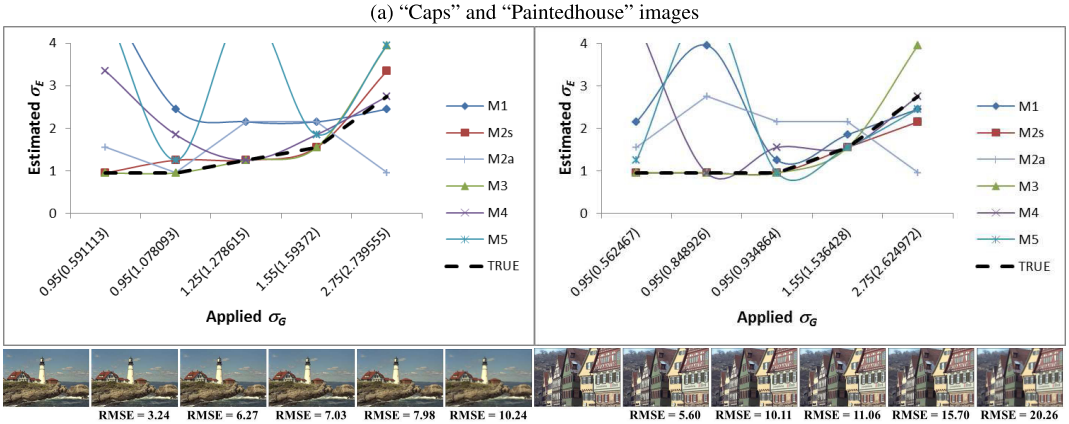

(b) "Lighthouse" and "Building" images

Fig. 9 Examples of estimation results by each metric. The thick dash line is the ground truth. In the x-axis, the values inside parentheses are the blur strengths given in the LIVE database and those outside parentheses are the mapped values. To quantify the image degradation, the root mean square error (RMSE) was given below each blurred image. The first image is the blur-free image.

Table 1 Blur strength estimation error.

Metric	$M1$	$M2s$	$M2a$	$M3$	$M4$	$M5$
Mean error	1.125	0.46	0.89	0.31	0.82	1.31

Table 2 Computation time of each metric for 768×512 images.

Metric	$M1$	$M2s$	$M2a$	$M3$	$M4$	$M5$
Time [μs]	18	16	16	72	70	17

et al. [13] and an improved version of the well-known NR-S metrics [14], [15], was applied to the same dataset and SVM framework. The results of Park's metric was compared to our best metric ($M3$). In results, the estimation error of Park's metric was 0.49 on average and higher than ours. Also, as shown in Fig. 10, the results of our metric were much more consistent with the ground truth than those of

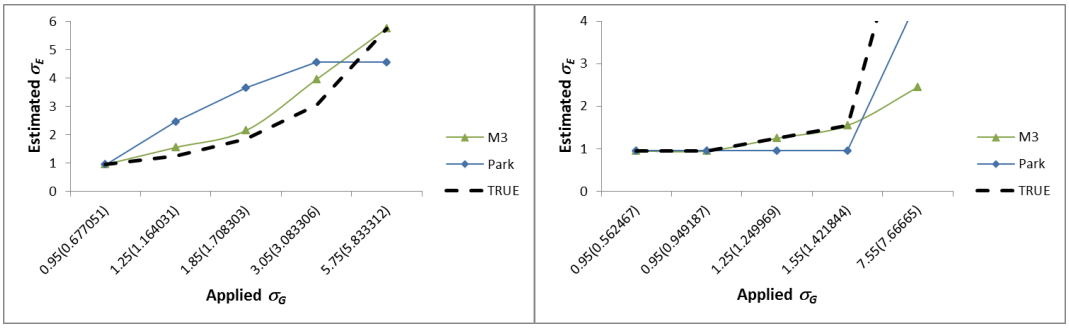

(a) "Caps" and "Paintedhouse" images

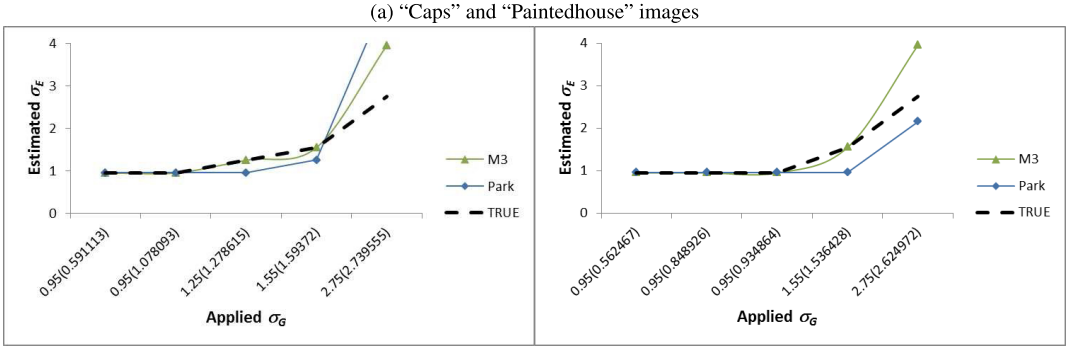

(b) "Lighthouse" and "Building" images

Fig. 10 Comparison of estimation results by our metric ($M3$) and Park's one.

the Park's one. Most of all, our metric was about 141 times faster than Park's one that took 10.15ms for 768×512 images.

4. Conclusion

In this letter, we proposed a no-reference blur estimation method in the frequency domain. After computing the CDF of the spectrum of blurred images and analyzing the relationship between its shape and the blur strength, we proposed six curve-shape analytic metrics for estimating blur strengths. Also, we employed an SVM-based learning scheme to improve the accuracy and robustness of the proposed metrics. Through experiments with Gaussian blurred images and comparison with a previous NR-S metric, we evaluated the performance of the proposed metrics. The results identified the superior metric.

In this letter, all the metrics were devised in a heuristic manner. In the future, we would like to devise a more theoretical metric and compare it with the heuristic ones.

References

[1] A. Mittal, A.K. Moorthy, and A.C. Bovik, "No-reference image quality assessment in the spatial domain," IEEE Trans. Image Process., vol.21, no.12, pp.4695–4708, 2012.
[2] R.W. Dosselmann and X.D. Yang, "No-reference noise and blur detection via the Fourier transform," Technical Report, University of Regina, Canada, CS-2012-01, 2012.
[3] B. Goossens, H. Luong, L. Platiša, and W. Philips, "Objectively measuring signal detectability, contrast, blur and noise in medical images using channelized joint observers," SPIE Medical Imaging, 2013.
[4] M. Dobes, L. Machala, and T. Fürst, "Blurred image restoration: A fast method of finding the motion length and angle," Digital Signal Process., vol.20, no.6, pp.1677–1686, 2010.
[5] W. Zhang and F. Bergholm, "Multi-scale blur estimation and edge type classification for scene analysis," Int. J. Comput. Vision, vol.24, no.3, pp.219–250, 1997.
[6] S. Dai and Y. Wu, "Motion from blur," Proc. CVPR, pp.1–8, 2008.
[7] R. Ferzli and L.J. Karam, "A no-reference objective image sharpness metric based on the notion of Just Noticeable Blur (JNB)," IEEE Trans. Image Process., vol.18, no.4, pp.717–728, 2009.
[8] M. Hollander and D. Wolfe, Nonparametric statistical methods, Wiley Series in Probability and Statistics - Applied Probability and Statistics Section, 1973.
[9] J. Shi, L. Xu, and J. Jia, "Discriminative blur detection features," Proc. CVPR, pp.2965–2972, 2014.
[10] C.C. Chang and C.J. Lin, "LIBSVM: A library for support vector machines," ACM Trans. Intell. Syst. Tech., vol.2, no.3, pp.1–27, 2011.
[11] http://live.ece.utexas.edu/research/quality/. LIVE database.
[12] http://opencv.willowgarage.com/wiki/. OpenCV.
[13] H. Park, H. Mitsumine, and M. Fujii, "A cost-effective and robust edge-based blur metric based on careful computation of edge slope," IEICE Trans. Inf. & Syst., vol.E94-D, no.9, pp.1834–1838, Sept. 2011.
[14] P. Marziliano, F. Dufaux, S. Winkler, and T. Ebrahimi, "A no-reference perceptual blur metric," Proc. ICIP, pp.57–60, 2002.
[15] G. Cao, Y. Zhao, and R. Ni, "Edge-based blur metric for tamper detection," J. Information Hiding and Multimedia Signal Processing, vol.1, no.1, pp.20–27, 2010.